Energy Efficiency Enhancement in Mini-Hydro-Power Pumping Systems Using the Improved Voltage Balancing of Modular Multilevel Converters

Dao Tuan Anh
College of Agricultural Mechanics, Phu Tho, Vietnam
tuanhbx@cam.edu.vn

Nguyen The Vinh
Automation and Robotics Laboratory (ARL), Posts and Telecommunications Institute of Technology, Hanoi, Vietnam
vinhnt@ptit.edu.vn

Van Thang Nguyen
Autonomous Vehicles and Intelligent Systems Laboratory (AVIS Lab), Posts and Telecommunications Institute of Technology, Hanoi, Vietnam
thangnv1@ptit.edu.vn (corresponding author)

Received: 26 September 2025 | Revised: 13 October 2025, 3 November 2025, and 18 November 2025 | Accepted: 3 December 2025

 DOI: https://doi.org/10.48084/etasr.15151

ABSTRACT

This paper proposes a mathematical estimation-based strategy for Submodule (SM) capacitor voltage balancing in Modular Multilevel Converters (MMCs), with the objective of suppressing circulating currents and improving energy efficiency in hydro pumping applications. The method derives the SM voltage reference from the estimated capacitor energy ripple instead of a fixed capacitor voltage reference, enabling adaptive suppression of circulating currents and improved energy efficiency. Simulation studies confirm that the method effectively balances capacitor voltages, suppresses circulating currents, and enhances current quality. Compared with the conventional balancing scheme, the proposed method reduces the Total Harmonic Distortion (THD) of arm currents from about 11% to 7% and increases converter efficiency from 93% to nearly 98% at rated load. The efficiency improvement becomes more evident under high-load conditions, confirming the scalability and adaptability of the proposed approach across various operating ranges. It enhances converter performance and reliability while significantly improving energy utilization. These advantages make the method a practical and efficient solution for MMC-based hydro pumping systems.

Keywords-improved submodule voltage balancing; submodule voltage ripple estimation; mini-hydropower pumping system; modular multilevel converter

I. INTRODUCTION

The MMC has become one of the most promising multilevel converter topologies for medium- and high-voltage applications. Its modular structure, high efficiency, excellent harmonic performance, and inherent redundancy make it superior to traditional two-level and three-level converters [1-3]. Owing to these advantages, MMCs have been widely deployed in various fields, including motor drives [4-6], High-Voltage Direct Current (HVDC) transmission systems [7-10], and flexible AC transmission systems such as Static Synchronous Compensators (STATCOMs) [11-13].

Despite these merits, MMCs face inherent challenges associated with circulating currents that flow within the converter arms due to voltage differences among the converter legs [14]. Although such currents do not directly affect the AC-side voltage or current waveforms, they lead to increased capacitor voltage ripple, higher semiconductor losses, and additional thermal stress, all of which reduce the overall efficiency and reliability of the system. To address these issues, significant research efforts have been dedicated to developing circulating current suppression strategies. For example, the combination of predictive control with proportional-resonant

regulators has been proposed to effectively reduce circulating components in Half-Bridge (HB)MMCs [15]. Passivity-based integral sliding mode control has also been introduced in multiphase wind power systems to suppress circulating harmonics with improved robustness [16]. For medium-voltage back-to-back MMCs, Lyapunov-function-based approaches have demonstrated substantial improvements in circulating current reduction [17]. Furthermore, improved Nearest Level Modulation (NLM) techniques have been shown to enhance output voltage quality and reduce harmonic distortion in MMC, while maintaining low computational complexity and practical feasibility for real-time implementation [18]. Collectively, these studies underscore the continuous progress in controlling circulating currents; however, most existing works concentrate on HVDC, wind energy conversion, or general grid-connected applications, whereas considerably less attention has been given to pumping systems, where MMCs could also provide significant benefits.

In mini-hydropower plants, pumping systems play a vital role in regulating reservoir water levels, supporting irrigation, and maintaining water supply for rural communities [19-22]. The operation of these pumps is characterized by the head–flow (H–Q) relationship, where the available water head decreases as the discharge flow increases. This nonlinear hydraulic behavior directly affects the motor torque and power demand, which vary significantly with changes in water level, flow rate, and seasonal conditions. As a result, variable-speed operation is required to maintain optimal pumping efficiency and system stability. These varying hydraulic loads place stringent performance requirements on the converter's dynamic response and efficiency. Conventional converter topologies, including two-level or NPC structures, often face difficulties under such conditions due to high switching losses, limited scalability, and poor harmonic performance. In contrast, the MMC offers excellent scalability, low harmonic distortion, and high efficiency, making it a promising and energy-efficient solution for variable-speed hydro-pump drives in modern mini-hydropower applications. Motivated by these challenges, the present study proposes an enhanced SM voltage balancing strategy specifically designed for MMC-based pumping systems in mini-hydropower plants. In conventional control schemes, the circulating current reference is generally derived from the output of a PI regulator acting on the deviation between the capacitor voltage reference and its measured value. Such an approach is inherently limited by the accuracy with which the reference voltage can approximate the actual capacitor dynamics, thereby introducing steady-state errors that propagate into the circulating current control loop. To overcome this limitation, the present work develops a refined mathematical model for SM capacitor voltage estimation, enabling a more precise generation of the circulating current reference. By aligning the reference more closely with the actual capacitor behavior, the proposed method effectively suppresses circulating currents, reduces internal losses, and enhances overall energy efficiency.

The validity of the approach is substantiated through comprehensive simulations in MATLAB/Simulink, confirming its effectiveness and practical deployment for mini-hydropower pumping systems. Additionally, Hardware-in-the-Loop (HIL) validation using OPAL-RT is planned for future work to further evaluate its real-time feasibility.

II. MODULAR MULTILEVEL CONVERTER

A. Operating Principle

The schematic of a three-phase MMC is illustrated in Figure 1. Each phase leg, also referred to as a converter arm, is split into an upper arm and a lower arm. The upper arm is connected to the positive DC bus, while the lower arm is connected to the negative DC bus. Each arm consists of N_{sm} identical SMs along with an arm inductor (L_{arm}), which serves to suppress circulating currents caused by voltage imbalances between the two arms. In this study, the SM is implemented as an HB cell, containing two IGBTs (S_1, S_2), their corresponding anti-parallel diodes, and a DC storage capacitor (C_{dc}).

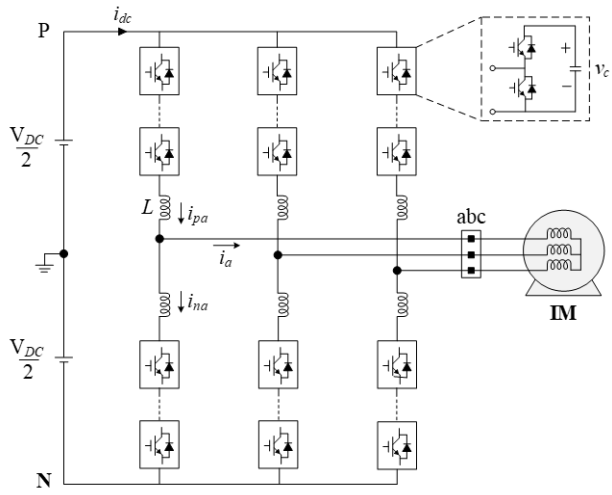

Fig. 1. Circuit configuration of a three-phase MMC.

For the analytical modeling and derivation of the proposed control strategy, the three-phase output voltages (v_{oj}) and currents (i_{oj}) of the MMC are assumed to be sinusoidal, balanced, and symmetrical under steady-state operating conditions [3]. The instantaneous phase voltages and currents can be expressed as:

$$\begin{cases} v_{oj} = V_j \cos\left(\omega t + \delta_j\right) \\ i_{oj} = I_j \cos\left(\omega t + \delta_j - \phi_j\right) \end{cases} \quad (1)$$

where v_{oj} and i_{oj} denote the instantaneous voltage and current of phase j (with j = a, b, c). The parameters V_j and I_j represent their respective amplitudes, while δ_j is the initial phase angle of each phase, typically set to $\delta_a = 0$, $\delta_b = 2\pi/3$, and $\delta_c = -2\pi/3$. The variable φ_j denotes the phase displacement between the voltage and current of phase j.

By applying Kirchhoff's Voltage Law (KVL) to each arm of the MMC, the instantaneous voltages of the upper arm and lower arm can be expressed, as shown in (2). Substituting the expressions of the three-phase output voltages and currents from (1) into the KVL equations allows the explicit analytical

forms of the upper-arm voltage v_{ju} and lower arm voltage v_{jl} to be derived, as given in:

$$\begin{cases} v_{ju} = \frac{1}{2}V_{DC} - v_{oj} \\ v_{jl} = \frac{1}{2}V_{DC} + v_{oj} \end{cases} \quad (2)$$

$$\begin{cases} v_{ju} = \frac{1}{2}V_{DC} - V_j \cos\left(\omega t + \delta_j\right) \\ v_{jl} = \frac{1}{2}V_{DC} + V_j \cos\left(\omega t + \delta_j\right) \end{cases} \quad (3)$$

where v_{ju} and v_{jl} denote the voltages of the upper and lower arms in phase j, and VDC is the total DC-link voltage.

Similarly, the instantaneous arm currents of each phase leg can be defined based on the current distribution between the converter arms, as presented in (4). The circulating current component, given in (5), represents the average of the upper- and lower-arm currents and primarily results from voltage imbalances between the converter arms as well as energy storage dynamics in the arm inductors and SM capacitors:

$$\begin{cases} i_{ju} = \frac{1}{2}i_{oj} + i_{cirj} \\ i_{jl} = -\frac{1}{2}i_{oj} + i_{cirj} \end{cases} \quad (4)$$

$$i_{cirj} = \frac{1}{2}\left(i_{ju} + i_{jl}\right) \quad (5)$$

where i_{ju} and i_{jl} are the upper and lower arm currents of phase j, while i_{cirj} denotes the corresponding circulating current.

B. Research Background on SM Capacitor Voltage Balancing

In conventional MMC control schemes, the circulating current reference of phase j (i^*_{cirj}) is typically derived from the regulation of the average SM capacitor voltage, as described in (6). In this classical approach, a Proportional–Integral (PI) controller adjusts the circulating current reference so that the measured average capacitor voltage tracks a fixed reference value, which corresponds to the rated SM capacitor voltage [14]. Although this method is simple and widely implemented, it inherently assumes that the reference capacitor voltage remains constant, irrespective of instantaneous load variations or arm energy fluctuations. This constant-reference assumption neglects the dynamic behavior of capacitor voltage ripples caused by the power exchange between the upper and lower arms, which results in incomplete circulating current suppression and increased energy imbalance among SMs. To overcome these limitations, the current study proposes a novel mathematical estimation–based capacitor voltage balancing method that adaptively updates the reference voltage according to real-time variations in the capacitor stored energy. Instead of relying on a static voltage reference, the proposed approach continuously estimates the instantaneous SM capacitor voltage ripple ($v^*_{phj,est}$) using the analytical model derived from arm power and energy dynamics. By aligning the voltage reference more closely with the true capacitor dynamics, the proposed strategy achieves precise suppression of circulating currents, minimizes unnecessary internal power exchange, and effectively equalizes the energy distribution among SMs.

$$i^*_{cirj} = \left(K_P + \frac{K_I}{s}\right)\left(V^*_C - \overline{V}_{Cj}\right) \quad (6)$$

III. PROPOSED ESTIMATION-BASED SM VOLTAGE BALANCING CONTROL

A. Mathematical Model of SM Capacitor Voltage Reference

Using the arm voltage expressions defined in (2) and the corresponding arm current definitions given in (4), the instantaneous power of the upper and lower arms, denoted as P_{ju} and P_{jl}, are formulated in (7) and further expanded in (8). These power expressions capture the instantaneous power transfer between the DC link and each converter arm, encompassing both the external AC power delivered to the load and the internal circulating power components within the MMC:

$$\begin{cases} P_{ju} = \left(\frac{1}{2}V_{DC} - v_{oj}\right)\left(\frac{1}{2}i_{oj} + i_{cirj}\right) \\ P_{jl} = \left(\frac{1}{2}V_{DC} + v_{oj}\right)\left(-\frac{1}{2}i_{oj} + i_{cirj}\right) \end{cases} \quad (7)$$

$$\begin{cases} P_{ju} = \frac{1}{2}V_{DC}i_{cirj} - \frac{1}{2}v_{oj}i_{oj} + \frac{1}{4}V_{DC}i_{oj} - v_{oj}i_{cirj} \\ P_{jl} = \frac{1}{2}V_{DC}i_{cirj} - \frac{1}{2}v_{oj}i_{oj} - \frac{1}{4}V_{DC}i_{oj} + v_{oj}i_{cirj} \end{cases} \quad (8)$$

where P_{ju} and P_{jl} represent the instantaneous power of the upper and lower arm in phase j, respectively.

Based on the power balance criteria between the DC side and the AC side of the converter, the circulating current i_{cirj} can be obtained as expressed in:

$$i_{cirj} = \frac{v_{oj}i_{oj}}{V_{DC}} \quad (9)$$

By substituting the expressions for the three-phase output voltages and currents from (1) and the decomposed power components from (9) into (8), the instantaneous power of the upper arm can be expressed explicitly as given in (10). To further quantify this behavior, the ripple component of the upper-arm power, $P_{ju,rpl}$, is integrated over time to obtain the corresponding energy ripple stored in the upper arm, denoted as $E_{ju,rpl}$, as expressed in (11). Similarly, by applying the same procedure to the lower arm, the lower-arm energy ripple, $E_{jl,rpl}$, is derived as given in (12). Based on (12) and (13), the total phase energy ripple in phase j, denoted as $E_{j,rpl}$, is obtained by taking the difference between the energy ripple of the upper and lower arms, as expressed in (14). This subtraction reflects the instantaneous energy imbalance between the two arms of the same phase, which is the main cause of capacitor voltage fluctuations within the converter:

$$P_{ju,rpl} = \left(\frac{V_{DC}}{4} - \frac{v_{oj}^2}{V_{DC}} \right) I_j \cos\left(\omega t + \delta_j - \phi_j \right) \quad (10)$$

$$E_{ju,rpl} = \left(\frac{V_{DC}}{4\omega} - \frac{v_{oj}^2}{\omega V_{DC}} \right) I_j \sin\left(\omega t + \delta_j - \phi_j \right) \quad (11)$$

$$E_{jl,rpl} = \left(-\frac{V_{DC}}{4\omega} + \frac{v_{oj}^2}{\omega V_{DC}} \right) I_j \sin\left(\omega t + \delta_j - \phi_j \right) \quad (12)$$

$$\begin{aligned} E_{j,rpl} &= E_{ju,\max} - E_{jl,\max} \\ &= \frac{V_{DC} I_j}{2\omega} \end{aligned} \quad (13)$$

$$\begin{aligned} E_{j,rpl} &= \left(\frac{1}{2} v_{c,\max}^2 - \frac{1}{2} v_{c,\min}^2 \right) \\ &= N_{sm} C_{dc} v_c \Delta v_{pp} \end{aligned} \quad (14)$$

Finally, by combining the analytical relationships established in (14) and (15), the peak-to-peak voltage ripple of the SM capacitor, denoted as Δv_{pp} is derived and presented in (15). Building upon this relation, the practical estimation of the SM capacitor voltage ripple is subsequently defined in (16), where $v_{phj,est}^*$ represents the estimated reference value for the SM capacitor voltage in phase *j*:

$$\Delta v_{pp} = \frac{I_j}{2C_{dc}\omega} \quad (15)$$

$$v_{phj,est}^* = v_{c,rated} + \Delta v_{pp} \quad (16)$$

B. Proposed Improved SM Capacitor Voltage Balancing

The presence of circulating current remains one of the most critical challenges affecting the system performance of the MMC. These internal currents flow between the upper and lower converter arms and, although they do not contribute to external load power, they lead to additional conduction and switching losses, increased capacitor voltage oscillations, and a consequent reduction in overall energy efficiency. Therefore, the accurate mitigation of such currents is essential to ensure stable operation and optimal utilization of stored energy in the SM capacitors. To address this problem, this paper proposes a novel estimation-based capacitor voltage balancing strategy in which the reference voltage of the SM capacitor is not treated as a constant but is dynamically estimated using the mathematical ripple model derived in (16).

Unlike conventional balancing methods, where the reference voltage is fixed at V_{dc}/N_{sm} and cannot reflect instantaneous arm energy variations, the proposed approach introduces an adaptive reference formulation that explicitly incorporates the capacitor voltage ripple component Δv_{pp}. This ripple term is computed from the estimated arm energy fluctuation $E_{j,rpl}$ providing a real-time representation of the converter's internal energy state. As a result, the MMC can continuously track and compensate for instantaneous arm energy imbalances, thereby suppressing the dominant components of circulating current that arise from the dynamic power exchange between converter arms.

The pseudo-code of the proposed dynamic voltage reference estimation is shown in Figure 2. Starting from the system parameters (V_{dc}, V_j, I_j, N_{sm}, C_{dc}), the instantaneous arm energy ripple ($E_{j,rpl}$) is estimated and used to compute the dynamic voltage reference $v_{phj,est}^*$. A supervisory decision stage monitors the circulating current amplitude to determine whether the suppression condition is satisfied. If the circulating current remains above the predefined threshold, the previous voltage reference is retained to maintain stability; otherwise, the optimized reference is updated for the next control cycle. This adaptive loop ensures both stability and responsiveness under varying load and modulation conditions.

Algorithm: Dynamic_voltage_reference_estimation

input: V_{dc}, v_j, i_j, N_{sm}, C_{dc}
output: Optimized dynamic voltage reference ($v_{phj,est}^*$)
start:
1 Compute upper- and lower-arm power:
$P_{ju}(t) \leftarrow v_{ju}(t).\, i_{ju}(t)$, $P_{jl}(t) \leftarrow v_{jl}(t).i_{jl}(t)$
2 Integrate power ripple to energy ripple:
3 $E_{ju,rpl}(t) \leftarrow \int P_{ju}(t)dt$, $E_{jl,rpl}(t) \leftarrow \int P_{jl}(t)dt$
4 Compute total phase energy ripple:
5 $E_{j,rpl}(t) \leftarrow E_{ju,rpl}(t) - E_{jl,rpl}(t)$
6 Estimate SM capacitor voltage ripple:
7 $\Delta v_{pp} \leftarrow f(E_{j,rpl}(t), C_{dc})$
8 Generate dynamic SM voltage reference:
$v_{phj,est}^* \leftarrow V_{dc}/N_{sm} + \Delta v_{pp}$
9 Circulating current suppression check:
if $(|i_{cir,j}(t)| \le i_{threshold})$ **then**
$v_C^*(t) \leftarrow v_{phj,est}^*(t)$
else $v_C^*(t) = v_C^*(t-1)$
End if
10 **Output** $v_{phj,est}^*$
End

Fig. 2. Pseudo-code of the proposed dynamic voltage reference estimation based on circulating current analysis.

As depicted in Figure 3, the proposed control structure integrates the average capacitor voltage regulation and individual SM voltage balancing loops, both driven by the estimated capacitor voltage reference derived from real-time arm energy ripple. This adaptive reference enables the controller to accurately follow capacitor dynamics, ensuring effective suppression of circulating currents and uniform voltage distribution among SMs. The estimation-based balancing loops are closely coordinated with the Field-Oriented Control (FOC), which manages dq-axis current regulation and overall power exchange with the motor or grid. Through PSPWM, the converter achieves uniform switching loss distribution, smooth output voltage synthesis, and enhanced overall energy efficiency under variable load conditions.

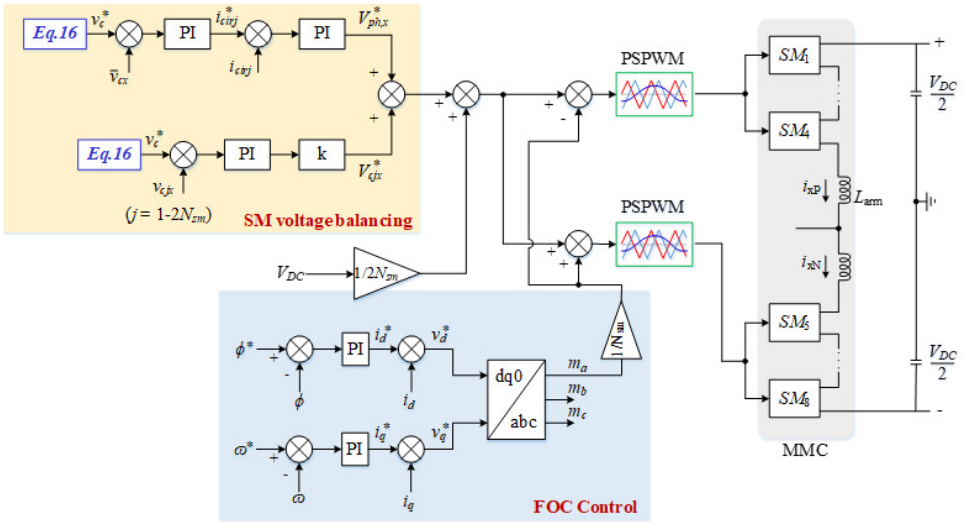

Fig. 3. Proposed improved SM capacitor voltage balancing control based on the estimated SM capacitor voltage ripple.

By embedding the circulating current suppression mechanism directly into the voltage balancing process, the proposed estimation-based control approach achieves simultaneous improvements in voltage stability, loss reduction, and overall energy efficiency. Simulation results confirm that this integrated scheme effectively minimizes arm current distortion, stabilizes SM capacitor voltages, and enhances converter efficiency by approximately 5% compared with conventional fixed-reference methods.

IV. SIMULATION RESULTS

The proposed circulating current reduction strategy was validated through time-domain simulations of an MMC-based hydro pumping system using the parameters outlined in Table I. The simulations were performed for a PMSM-driven hydro-pumping system rated at 4160 V, 250 A, 1000 rpm, and 5300 Nm. The representative machine and control parameters are Rs = 0.02 Ω, L_d = 2.5 mH, L_q = 2.7 mH, λ_{pm} = 3.33 Wb, J = 20 kg.m^2, B = 0.1 Nms/rad, with a standard PI anti-windup structure.

Figure 4 shows that the estimated reference accurately tracks the actual capacitor voltages, maintaining balanced fluctuations between SMs. This confirms that the proposed model provides precise voltage reference estimation and stable capacitor voltage distribution. When the conventional SM voltage balancing method is applied, as displayed in Figure 5, the arm currents exhibit considerable distortion due to the presence of circulating currents. The circulating current responses confirm that large oscillatory components are introduced into the arms, leading to high THD levels of 11.2% and 11.5% for the upper and lower arms, respectively. In contrast, the results in Figure 6 demonstrate that the proposed estimation-based method significantly improves the current waveforms. The arm currents become more sinusoidal, while the circulating current components are effectively suppressed. Consequently, the THD values are reduced to 7.2% and 7.5%, representing a substantial improvement compared with the conventional approach.

TABLE I. SYSTEM PARAMETERS

Parameter	Symbol	Value
DC-link voltage	V_{DC}	7000 V
Number of SMs per arm	N_{sm}	4
Arm inductance	L_{arm}	1.5 mH
SM capacitance	C_{dc}	1500 µF
Switching frequency	f_{sw}	2000 Hz
Rated motor voltage	V_{rated}	4160 V
Rated motor current	I_{rated}	250 A
Rated motor speed	ω_{rated}	1000 rpm
Rated motor torque	T_{rated}	5300 Nm

To evaluate the dynamic robustness of the proposed estimation-based control, additional simulations were performed with step changes in load torque, representing variations in hydraulic head. Figure 7 shows that when the load increases or decreases at t = 0.2 s, the circulating current exhibits short transients but rapidly returns to its steady-state value within one fundamental cycle. A DC-link voltage dip scenario was simulated to examine converter performance under severe operating disturbances. Such voltage drops frequently occur in grid-connected or hydro-pumping systems due to load transients or grid faults, making them a relevant test of controller resilience. Figure 8 illustrates the converter response when the DC-link voltage suddenly reduces from 7000 V to 5000 V at t = 0.30 s. As portrayed in Figure 8(a), the upper- and lower-arm currents i_{au}, i_{al} show a transient distortion immediately after the voltage dip but remain bounded and rapidly recover to a stable operating condition. Figure 8(b) presents the circulating current i_{cira} and its reference i^*_{cira}. The DC voltage dip leads to relatively high THD levels of 12.1% and 11.3% for the upper and lower arms, respectively, as depicted in Figure 8(c). The proposed estimation-based balancing controller promptly compensates for the disturbance,

limiting the overshoot to about 20% of the steady-state amplitude and restoring steady operation within approximately 0.06 s, as shown in Figure 8(b). Additional robustness tests were carried out under sudden variations of the DC capacitor and arm inductor.

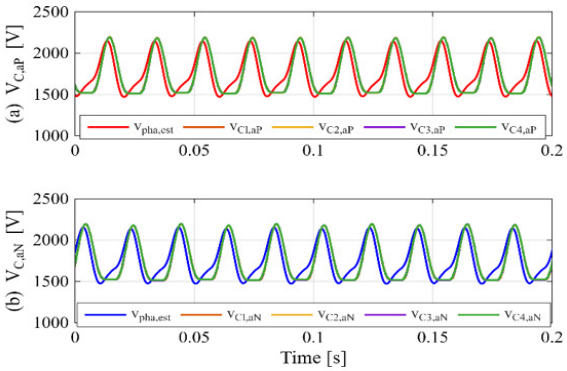

Fig. 4. Simulated SM capacitor voltage waveforms of: (a) upper and (b) lower arms using the proposed estimation-based control.

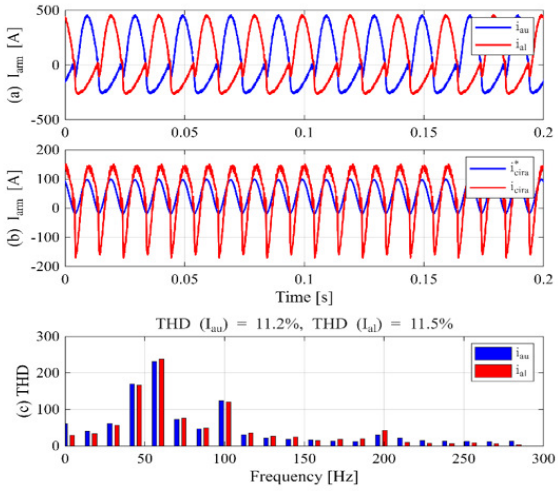

Fig. 5. Responses of the conventional SM voltage balancing method [14]: (a) arm currents, (b) circulating currents, (c) THD of arm currents.

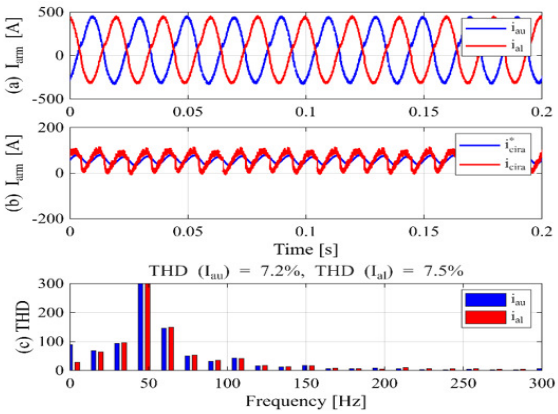

Fig. 6. Performance of the proposed improved SM voltage balancing control: (a) arm currents, (b) circulating currents, (c) THD of arm currents.

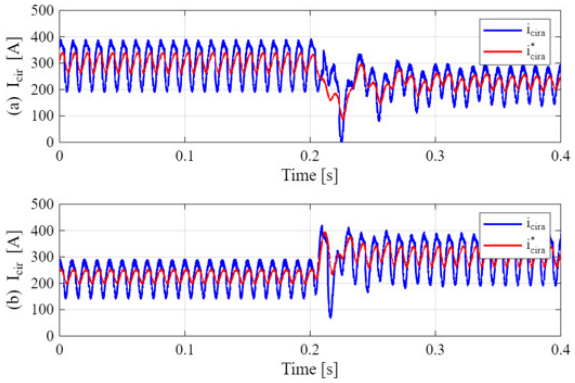

Fig. 7. Dynamic responses of the circulating current under variable-load conditions: (a) load increase, (b) load decrease.

TABLE II. LOSS MODEL

Loss component	Symbol	Calculation method
IGBT conduction	$P_{cond,IGBT}$	$P_{cond,IGBT}$
Diode conduction	$P_{cond,D}$	$P_{cond,D}$
Switching loss	P_{sw}	P_{sw}
Capacitor ESR loss	P_{ESR}	$I^2_{C,rms}R_{ESR}$
Arm copper loss	P_{cu}	$I^2_{arm,rms}R_{arm}$
Control overhead	P_{ctrl}	0.3% P_{rated}

As displayed in Figure 9, reducing C_{dc} by 30% at t = 0.10 s produces a short circulating current transient with about 25% overshoot and a settling time of roughly one cycle, while the RMS value quickly returns to nominal. Increasing L_{arm} by 30% at t = 0.20 s results in a smaller overshoot (≈20%) and similar settling behavior. In the steady-state interval (t ≥ 0.20 s), the arm-current THD remains low (≈6.1% and 5.5%), confirming that the proposed method preserves current quality and maintains stable operation even under substantial parameter deviations.

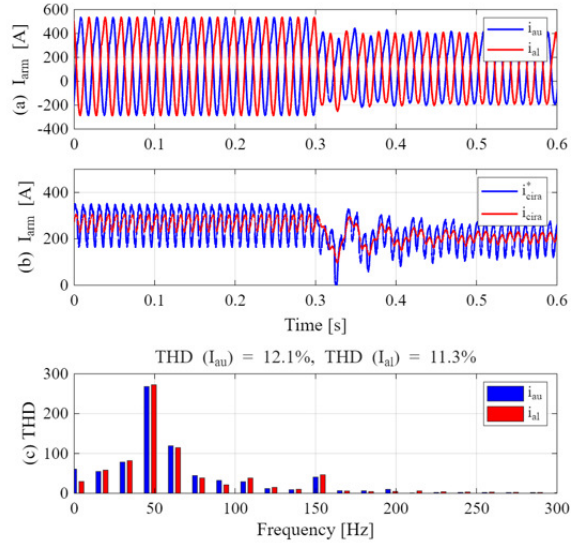

Fig. 8. Dynamic response under DC-link voltage dip: (a) arm currents, (b) circulating currents, (c) THD of arm currents.

The benefits of the proposed method are also reflected in the overall converter efficiency. As shown in Figure 10, the proposed scheme maintains higher efficiency across the entire load range and reaches nearly 98% at rated load, compared to about 93% for the conventional method [14]. The efficiency gap widens as load increases because circulating-current suppression becomes more impactful at medium and high-power levels. Under rated conditions, the proposed controller yields an absolute improvement of approximately 5%, confirming its suitability for hydro-pumping systems with varying load demands. To demonstrate practical relevance, a simplified hydraulic model (H–Q and η–Q) and a typical 24-h operating profile were combined with the efficiencies in Figure 10, resulting in an estimated 5.1% daily energy saving, as detailed in Appendix A.

To enhance transparency in efficiency evaluation, Table II summarizes all loss components considered in the converter model, including conduction, switching, ESR, arm copper, and control overhead. The MMC employs Infineon FF600R17ME4 IGBT modules (1700 V, 600 A) operating at a switching frequency of 2 kHz. Switching losses were computed from datasheet energy-per-event parameters (Eon, Eoff, Erecovery) scaled by the simulated RMS current. The total converter efficiency was evaluated as expressed in:

$$\eta = \frac{P_{out}}{P_{out} + P_{cond} + P_{sw} + P_{ESR} + P_{cu} + P_{ctrl}} \quad (17)$$

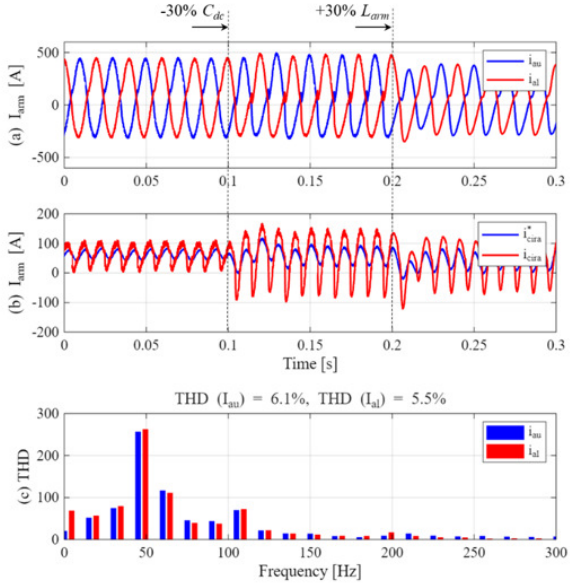

Fig. 9. Dynamic response under variations of the DC capacitor and arm inductance: (a) arm currents, (b) circulating currents, (c) arm-current THD.

TABLE III. COMPARATIVE ANALYSIS OF CIRCULATING CURRENT SUPPRESSION METHODS

Criterion	**MPC / optimization-based control [23, 24]**	**Passive harmonic filtering (2nd–4th order) [25]**	**Proposed estimation-based voltage balancing**
Main control principle	Predictive or optimization-based current and voltage regulation	Harmonic attenuation using tuned LC filters	Adaptive SM voltage reference estimation
Implementation complexity	Very high – requires precise modeling and heavy computation	Low – simple passive components	Moderate
Adaptability to load variation	Limited by model accuracy	Fixed tuning; poor adaptability	High – dynamically adjusts reference
Circulating current suppression	High, but computationally costly	Indirect and limited	High – achieved via real-time ripple estimation
Suitability for mini-hydro systems	Limited due to complexity and cost	Limited due to size and maintenance	Highly suitable; low-cost, scalable, adaptive

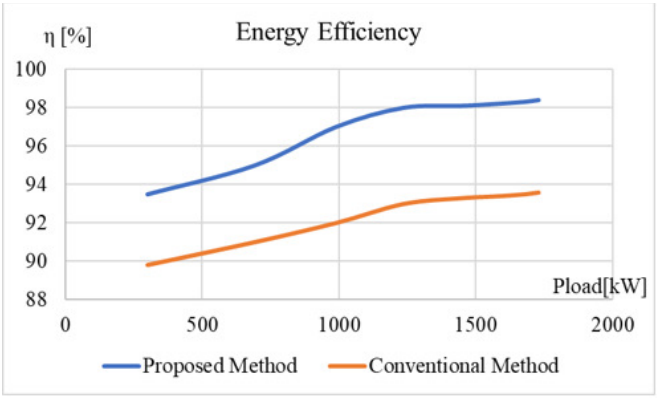

Fig. 10. Comparison of overall converter efficiency versus load power between the proposed estimation-based control and the conventional balancing method [14].

V. DISCUSSION

A. Economic Feasibility and Practical Adoption

Although MMCs were initially designed for high-voltage systems, advances in SiC and IGBT technology have reduced their cost and size, making them suitable for medium-voltage (3–10 kV) drives below 1 MW [10]. In hydro-pumping applications, the MMC modularity and redundancy enhance reliability and reduce maintenance downtime, offsetting the higher initial cost. Lifecycle analyses also show that MMCs offer lower total ownership cost than conventional inverters due to higher efficiency and reduced thermal stress [26].

B. Scalability and Implementation Aspects

The modular MMC structure enables easy scalability by varying the number of SMs per arm, allowing the same control framework across different power levels. Because the proposed control is purely estimation-based and requires no extra sensors

or filters, it can be readily implemented in simulation and real-time platforms such as OPAL-RT.

C. Comparative Performance and Practical Feasibility

Table III compares the proposed estimation-based control with MPC and Passive Filtering. Passive LC filters reduce low-order harmonics but are bulky and unsuitable for variable loads [25], while predictive control offers accuracy at high computational cost [23, 24]. The proposed method provides a practical compromise—achieving adaptive harmonic suppression and circulating current reduction without additional hardware, making it well suited for MMC-based hydro-pumping systems.

D. Limitations and Future Work

While simulation results are promising, several non-ideal hardware effects—such as switching delay, semiconductor drift, and capacitor tolerances—may affect voltage estimation accuracy. Furthermore, the present study simplified the hydraulic behavior by emulating variable load torque, rather than modeling the full nonlinear H–Q characteristics. Future work will address these aspects through HIL testing and prototype validation using an OPAL-RT platform, with the aim of refining both the estimation algorithm and its integration with a realistic hydro-turbine for MMC-based mini-hydropower applications.

TABLE IV. SYMBOLS AND UNITS

Symbol	Description	Unit
V_{dc}	Dc-link voltage	V
V_{ju}, v_{jl}	Upper and lower arm voltages of phase *j*	V
I_{ju}, i_{jl}	Upper and lower arm currents of phase *j*	A
$I_{cir,j}$	Circulating current of phase *j*	A
L_{arm}	Arm inductance	H
C_{dc}	SM capacitor	F
$E_{ju,rpl}$, $E_{jl,rpl}$	Energy ripple in upper/lower arm of phase *j*	J
Δv_{pp}	Peak-to-peak capacitor voltage ripple	V
N_{sm}	Number of SMs per arm	-
f_{sw}	Switching frequency	Hz
P_{ju}, p_{jl}	Power of upper and lower arms	W
η	Converter efficiency	%

VI. CONCLUSIONS

This study proposed a mathematical estimation-based strategy for Submodule (SM) voltage reference generation in Modular Multilevel Converters (MMCs) for hydro pumping systems. By adaptively reducing the circulating current reference, the method effectively suppresses circulating currents and improves arm current quality. Simulation results show a Total Harmonic Distortion (THD) reduction from about 11% to 7% and an efficiency increase of nearly 5%, reaching 98% at rated load. These results confirm that the proposed control enhances MMC performance and enables higher energy efficiency in practical hydro pumping applications.

ACKNOWLEDGMENTS

The research teamgratefully acknowledges the Posts and Telecommunications Institute of Technology, Hanoi, Vietnam for creating favorable conditions during the implementation of the research content of this article.

REFERENCES

[1] S. Debnath, J. Qin, B. Bahrani, M. Saeedifard, and P. Barbosa, "Operation, Control, and Applications of the Modular Multilevel Converter: A Review," *IEEE Transactions on Power Electronics*, vol. 30, no. 1, pp. 37–53, Jan. 2015, https://doi.org/10.1109/TPEL.2014.2309937.

[2] M. Saeedifard and R. Iravani, "Dynamic Performance of a Modular Multilevel Back-to-Back HVDC System," *IEEE Transactions on Power Delivery*, vol. 25, no. 4, pp. 2903–2912, Oct. 2010, https://doi.org/10.1109/TPWRD.2010.2050787.

[3] M. Hagiwara, R. Maeda, and H. Akagi, "Control and Analysis of the Modular Multilevel Cascade Converter Based on Double-Star Chopper-Cells (MMCC-DSCC)," *IEEE Transactions on Power Electronics*, vol. 26, no. 6, pp. 1649–1658, June 2011, https://doi.org/10.1109/TPEL.2010.2089065.

[4] D. D. Le and D.-C. Lee, "Current Stress Reduction and Voltage Total Harmonic Distortion Improvement of Flying-Capacitor Modular Multilevel Converters for AC Machine Drive Applications," *IEEE Transactions on Industrial Electronics*, vol. 69, no. 1, pp. 90–100, Jan. 2022, https://doi.org/10.1109/TIE.2021.3050394.

[5] V.-T. Nguyen, J.-W. Kim, J.-W. Park, J.-M. Lee, and B.-G. Park, "A modified submodule of modular multilevel converter using active power decoupling method for reducing capacitor voltage ripple under low-frequency operation," *IET Power Electronics*, vol. 16, no. 5, pp. 868–882, Apr. 2023, https://doi.org/10.1049/pel2.12432.

[6] J. Zhao, S. Huang, and Y. Xing, "Low- and high-speed control strategy for PMSM drive system based on MMC," *CPSS Transactions on Power Electronics and Applications*, pp. 1–10, 2025, https://doi.org/10.24295/CPSSTPEA.2025.00030.

[7] N. R. Karaka, I. C. Rath, and A. Shukla, "Modular Multilevel Converter and Parallel Hybrid Converter Based Open-End Windings AC Machine Drive for Wide Speed Range," *IEEE Transactions on Power Electronics*, vol. 41, no. 2, pp. 1811–1825, Feb. 2026, https://doi.org/10.1109/TPEL.2025.3602463.

[8] J. Yan, X. Shi, T. Liu, Z. Wang, L. Zhang, and L. Lin, "Weak Grid Characteristic Analysis and Operating Mode Selection for Voltage Support Enhancement of Wind Farms Connected to MMC-HVDC During Asymmetric Faults," *IEEE Transactions on Power Electronics*, vol. 41, no. 2, pp. 2629–2647, Feb. 2026, https://doi.org/10.1109/TPEL.2025.3613420.

[9] M. Usman, I. Kwon, and B.-W. Lee, "Valve-Side Single-Phase-to-Ground Fault Clearance in Bipolar Hybrid-MMC HVDC Systems Utilizing Thyristor Commutation Branches and Mechanical Interrupter," *IEEE Access*, vol. 13, pp. 166630–166648, 2025, https://doi.org/10.1109/ACCESS.2025.3612191.

[10] Z. Li, K. Jia, T. Bi, and J. Sun, "Adaptive Current Limit Control for Half-Bridge MMC-HVDC Single Pole-to-Ground Fault," *IEEE Transactions on Power Electronics*, vol. 41, no. 2, pp. 2452–2462, Feb. 2026, https://doi.org/10.1109/TPEL.2025.3602447.

[11] E. Ramakrishna, G. Jayakrishna, and S. Peddakotla, "Exploration of the HBSM MMC Five-Level Inverter for D-STATCOM Application," *Engineering, Technology & Applied Science Research*, vol. 13, no. 4, pp. 11191–11196, Aug. 2023, https://doi.org/10.48084/etasr.5965.

[12] E. Ramakrishna, J. Gadhamappagari, and P. Sujatha, "Auto tuning of PI Gains using Cuttlefish Optimization for DC Link Voltage Control in a 5-level HB MMC D-STATCOM," *Engineering, Technology & Applied Science Research*, vol. 13, no. 6, pp. 12086–12091, Dec. 2023, https://doi.org/10.48084/etasr.6413.

[13] R. O. de Sousa, A. F. Cupertino, L. M. F. Morais, H. A. Pereira, and R. Teodorescu, "Experimental Validation and Reliability Analyses of Minimum Voltage Control in Modular Multilevel Converter-Based STATCOM," *IEEE Transactions on Industrial Electronics*, vol. 71, no. 7, pp. 6546–6555, July 2024, https://doi.org/10.1109/TIE.2023.3303634.

[14] V.-T. Nguyen, J.-W. Kim, J.-W. Lee, and B.-G. Park, "Optimal Design of a Submodule Capacitor in a Modular Multilevel Converter for Medium Voltage Motor Drives," *Energies*, vol. 17, no. 2, 2024, Art. no. 471, https://doi.org/10.3390/en17020471.

[15] J. Li, Z. Zhang, Z. Li, and O. Babayomi, "Predictive Control of Modular Multilevel Converters: Adaptive Hybrid Framework for Circulating Current and Capacitor Voltage Fluctuation Suppression," *Energies*, vol. 16, no. 15, 2023, Art. no. 5772, https://doi.org/10.3390/en16155772.

[16] Y. Sang *et al*., "Passivity-based sliding mode current control for grid-following modular multilevel converter with system disturbances," *International Journal of Electrical Power & Energy Systems*, vol. 162, Nov. 2024, Art. no. 110222, https://doi.org/10.1016/j.ijepes.2024.110222.

[17] L. Fang, X. Xu, and T. Tarasiuk, "Research on Stability of MMC-Based Medium Voltage DC Bus on Ships Based on Lyapunov Method," *IEICE Transactions on Electronics*, vol. E105-C, no. 11, pp. 675–683, Nov. 2022.

[18] L. Lin, Y. Lin, Z. He, Y. Chen, J. Hu, and W. Li, "Improved Nearest-Level Modulation for a Modular Multilevel Converter With a Lower Submodule Number," *IEEE Transactions on Power Electronics*, vol. 31, no. 8, pp. 5369–5377, Aug. 2016, https://doi.org/10.1109/TPEL.2016.2521059.

[19] A. Barbón, F. González-González, L. Bayón, and R. Georgious, "Variable-Speed Operation of Micro-Hydropower Plants in Irrigation Infrastructure: An Energy and Cost Analysis," *Applied Sciences*, vol. 13, no. 24, Jan. 2023, Art. no. 13096, https://doi.org/10.3390/app132413096.

[20] R. Z. Falama, W. Skarka, and S. Y. Doka, "Optimal Design and Comparative Analysis of a PV/Mini-Hydropower and a PV/Battery Used for Electricity and Water Supply," *Energies*, vol. 16, no. 1, 2023, Art. no. 307, https://doi.org/10.3390/en16010307.

[21] M. Rumbayan and R. Rumbayan, "Feasibility Study of a Micro Hydro Power Plant for Rural Electrification in Lalumpe Village, North Sulawesi, Indonesia," *Sustainability*, vol. 15, no. 19, 2023, Art. no. 14285, https://doi.org/10.3390/su151914285.

[22] A. Barbón, F. González-González, L. Bayón, and R. Georgious, "Variable-Speed Operation of Micro-Hydropower Plants in Irrigation Infrastructure: An Energy and Cost Analysis," *Applied Sciences*, vol. 13, no. 24, 2023, Art. no. 13096, https://doi.org/10.3390/app132413096.

[23] X. Gao et al., "Modulated Model Predictive Control of Modular Multilevel Converters Operating in a Wide Frequency Range," IEEE Transactions on Industrial Electronics, vol. 70, no. 5, pp. 4380–4391, May 2023, https://doi.org/10.1109/TIE.2022.3183354.

[24] W. Zhang, G. Tan, X. Zhang, Q. Wang, and J. Zhang, "Optimal Switching Sequence Model Predictive Control for Modular Multilevel Converter," IEEE Transactions on Industrial Electronics, vol. 70, no. 6, pp. 5474–5483, June 2023, https://doi.org/10.1109/TIE.2022.3194599.

[25] B. Zhang and H. Nademi, "Modeling and Harmonic Stability of MMC-HVDC With Passive Circulating Current Filters," IEEE Access, vol. 8, pp. 129372–129386, 2020, https://doi.org/10.1109/ACCESS.2020.3009331.

[26] J. van Ammers, G. Ye, A. Lekić, B. Mihić, and M. Popov, "MMC Control Strategy for Converter Lifetime Optimization Based on Thermal Stress Analysis of Lower IGBT Device in Half-Bridge Submodules," *IEEE Transactions on Power Delivery*, vol. 40, no. 5, pp. 2671–2682, Oct. 2025, https://doi.org/10.1109/TPWRD.2025.3588731.

APPENDIX A

A simplified hydraulic model was added to link the converter performance to the mini-hydropower pumping system. The pump head–flow relation and the hydraulic power are approximated as expressed in:

$$H(Q) = H_0 - kQ^2 \tag{18}$$

$$P_{hyd} = \rho g Q H(Q) \tag{19}$$

where H_0 represents the shut-off head (m), Q is the discharge capacity (m^3/s), and k is the loss coefficient (ms^2/m^6), with ρ = 1000 kg/m^3 and g = 9.81m/s^2. The pump efficiency follows a quadratic curve:

$$\eta(Q) = a_0 + a_1 Q + a_2 Q^2 \tag{20}$$

A 24-h operating profile typical of irrigation systems (low load at night, two daily peaks at 80‑90%) was used to estimate energy consumption. Using the converter efficiencies obtained from Figure 10 (baseline ≈ 93%, proposed ≈ 98%), the estimated saving is calculated as in:

$$1 - \frac{0.93}{0.98} \approx 0.51\% \tag{21}$$

Assuming a 10 kW rated hydropower, pumping station operating 24 h per day at an average 90 % load, the daily hydraulic energy is about 216 kWh. Applying this 5.1% saving gives an energy reduction of ≈ 11 kWh/day, or ≈ 3.3 MWh/year.